RESEARCH ARTICLE

Key Points:
- Bed forms in the proposed 2016 ExoMars landing site form a complex pattern
- We describe a new type of wind streak formed by megaripples
- Changes in the wind direction were common in Meridiani Planum

Evidence for different episodes of aeolian construction and a new type of wind streak in the 2016 ExoMars landing ellipse in Meridiani Planum, Mars

S. Silvestro[1], D. A. Vaz[2,3], G. Di Achille[4], I. C. Popa[1], and F. Esposito[1]

[1]Istituto Nazionale di Astrofisica, Osservatorio Astronomico di Capodimonte, Napoli, Italy, [2]Centre for Geophysics of the University of Coimbra, Observatório Astronómico da Universidade de Coimbra, Almas de Freire, Coimbra, Portugal, [3]Instituto Superior Técnico, Centre for Natural Resources and the Environment, Lisboa, Portugal, [4]INAF-Osservatorio Astronomico di Teramo, Teramo, Italy

Abstract We present evidence for a complex, multigenerational bed form pattern and a new type of wind streak (the ripple streak) in the landing site ellipse of the 2016 ExoMars Entry descent and landing Demonstrator Module (EDM) in Meridiani Planum (Mars). We identified three main groups of bright-toned bed forms. Population 3, represented by NE-SW trending bed forms located inside craters, was emplaced by winds coming from the NW or the SE. Population 2, emplaced by strong easterlies, formed by intracrater transverse aeolian ridges (TARs) and N-S trending megaripples (plains ripples). Population 1 consists of a relict bed form pattern emplaced by winds coming from the north or south. Alternatively, population 1 can represent a sand ribbon pattern that formed together with the plain ripples. We also report the presence of a new type of wind streak, the ripple streak, which is formed by the population 2 bed forms clustered in the wake zone of impact craters. Based on the results of this work, we now know the EDM module is set to land in a complex aeolian environment. Data from the Dust Characterization, Risk Assessment, and Environment Analyser on the Martian Surface onboard the EDM can help to better decipher the wind regime in Meridiani Planum.

1. Introduction and Study Area

Wind is the main driver of surface erosion on Mars in the present-day atmospheric setting. Wind action was likely even more important in the past when the atmosphere of Mars was probable thicker than today [*Jakosky and Phillips*, 2001]. Meridiani Planum, the selected landing area for the ExoMars 2016 landing (Figure 1), is a key area to understand wind/surface interactions [*Sullivan et al.*, 2005; *Arvidson et al.*, 2006; *Golombek et al.*, 2006, 2010; *Squyres et al.*, 2006; *Balme et al.*, 2008; *Hayes et al.*, 2011]. During the Noachian epoch, unconsolidated material likely derived from basalt was accumulated by the wind into sand sheets and dunes in an environment with a fluctuating water table [*Arvidson et al.*, 2006]. The diagenetic processes led to the formation of the sedimentary rock unit described as "Burns Formation," which precipitated the sulfate cement under acidic ground water conditions [*Grotzinger et al.*, 2005; *McLennan et al.*, 2005]. The presence of the hematite concretions, ("blueberries") associated with these deposits are interpreted as aeolian lags that concentrated on the surface as the softer sulfate-rich sedimentary rocks were eroded away by the wind [*Arvidson et al.*, 2004; *Grotzinger et al.*, 2005; *McLennan et al.*, 2005; *Squyres et al.*, 2006].

In the present-day atmospheric setting, wind activity drives sand dune movement and wind streak formation [*Geissler et al.*, 2010, 2013; *Chojnacki et al.*, 2011, 2014; *Silvestro et al.*, 2011; *Bridges et al.*, 2013; *Fenton et al.*, 2015]. The results of wind action are visible on the surface, with the landscape in Meridiani Planum being dominated by the presence of vast fields of aeolian bed forms that have accumulated inside impact craters and on the surrounding plain [*Balme et al.*, 2008; *Arvidson et al.*, 2011]. Light-toned bed forms located inside craters are commonly referred as transverse aeolian ridges (TARs) [*Balme et al.*, 2008; *Bourke et al.*, 2010], while features on the plain have been called "plain ripples" [*Sullivan et al.*, 2005]. NASA Mars Exploration Rover (MER) Opportunity data showed that plain ripples interior consist of 100–300 μm sand. Their crest is armored with larger 1–2 mm hematite grains, which prevent them from being activated in the current climatic setting [*Jerolmack et al.*, 2006; *Squyres et al.*, 2006; *Weitz et al.*, 2006; *Golombek et al.*, 2010; *Arvidson et al.*, 2011]. TARs and plains ripples are widespread in the ESA ExoMars 2016 landing site ellipse, located between 5°W and 7°W, 0° and 3°S in the hematite-bearing plains of Terra Meridiani (Figure 1). In this work we show that these features have a complex spatial arrangement and we address such complexity by mapping
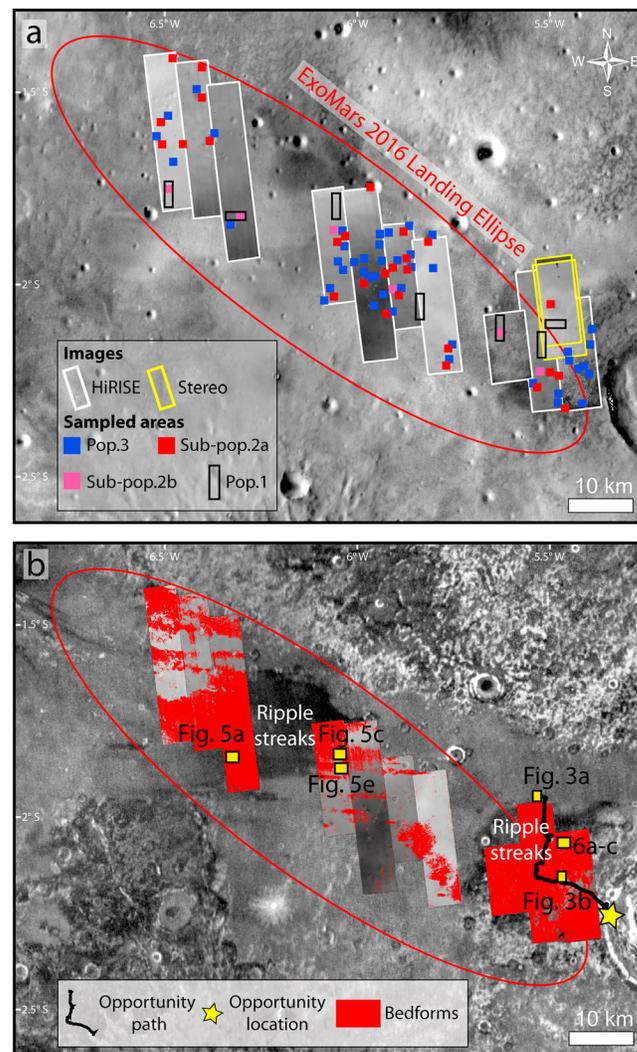
Figure 1. Study area. (a) Location map for the sampled crestline lengths and wavelengths. (b) Bed form location mapped in automatic (red areas) (THEMIS IR daytime (up) and nighttime (down) mosaics).

ripple distribution and by distinguishing different populations using geomorphic and statistic criteria [*Kocurek and Ewing*, 2005; *Beveridge et al.*, 2006; *Ewing et al.*, 2006, 2010; *Derickson et al.*, 2008]. We then illustrate the progressive construction of the complex pattern, and we discuss the wind regime associated with each constructional event. The derived wind directions are then compared with the orientations of the active wind streaks mapped throughout the study area. In addition, we report the presence of a new type of wind streak and we discuss the implications for the ESA ExoMars 2016 mission.

2. Methods

We mapped aeolian bed form occurrence in the ExoMars 2016 landing ellipse in 10 images acquired by the High Resolution Imaging Science Experiment (HiRISE) camera [*McEwen et al.*, 2007]. Images were coregistered over a regional 100 m/pixel infrared (IR) mosaic (daytime and nighttime) acquired by the Mars Odyssey Thermal Emission Imaging System (THEMIS) [*Christensen et al.*, 2004] (Figure 1 and Table 1). Aeolian bed forms were mapped using both automatic and manual approaches (Figures 1a and 1b). An automatic object-based bed form mapping technique [*Vaz and Silvestro*, 2014] was used to map bed form locations in the study area (Figure 1b).

This approach consists of the automatic delineation and characterization of bed forms traces. The obtained line segments are used to generate a regular grid (with 25 m spacing between nodes) for which average wavelengths are computed, enabling the regional assessment of bed form wavelength spatial distribution.

We manually traced the bed form crestlines on selected areas throughout the landing ellipse in ArcGIS (Figure 1a). We visually identified different populations by looking at bed form trends, lengths, wavelengths, and superposition relationships. Bed form length and wavelength have been extracted (Figure 2) and combined with trend measurements to statistically segregate the different populations visually identified on HiRISE [*Beveridge et al.*, 2006; *Ewing et al.*, 2006, 2010]. In order to derive the present-day wind directions, we manually mapped the bright and dark wind streaks as in Figure 3.

Bed form height is computed on a digital terrain model (DTM) having a spatial resolution = 1 m/pixel and a vertical precision of 0.30 m [*Kirk et al.*, 2003; *Okubo*, 2010]. The DTM was built using the NASA Ames Stereo Pipeline [*Moratto et al.*, 2010] from one HiRISE stereo couple on the SE landing ellipse (Figure 4 and Table 1). Topographic data helped to identify the population 1 pattern by highlighting its topographic signature.

Table 1. HiRISE Images Used in This Work

HiRISE ID	Acquisition Date	Latitude (Centered)	Longitude (East)	Stereo (y/n)
ESP_020758_1780	30 December 2010	−2.179°	354.565°	n
ESP_016644_1780	13 February 2010	−2.145°	354.477°	n
ESP_033786_1780	11 October 2013	−2.162°	354.383°	n
ESP_034775_1780	27 December 2013	−2.055°	354.200°	n
PSP_003511_1780	27 April 2007	−1.979°	354.112°	n
ESP_033351_1780	07 September 2013	−1.975°	354.025°	n
ESP_034274_1780	18 November 2013	−1.899°	353.933°	n
ESP_034986_1785	12 January 2014	−1.705°	353.671°	n
ESP_032784_1785	25 July 2013	−1.622°	353.586°	n
ESP_027193_1785	15 May 2012	−1.604°	353.504°	n
ESP_022380_1780	06 May 2011	−2.066°	354.522°	y
ESP_021747_1780	18 March 2011	−2.043°	354.519°	y
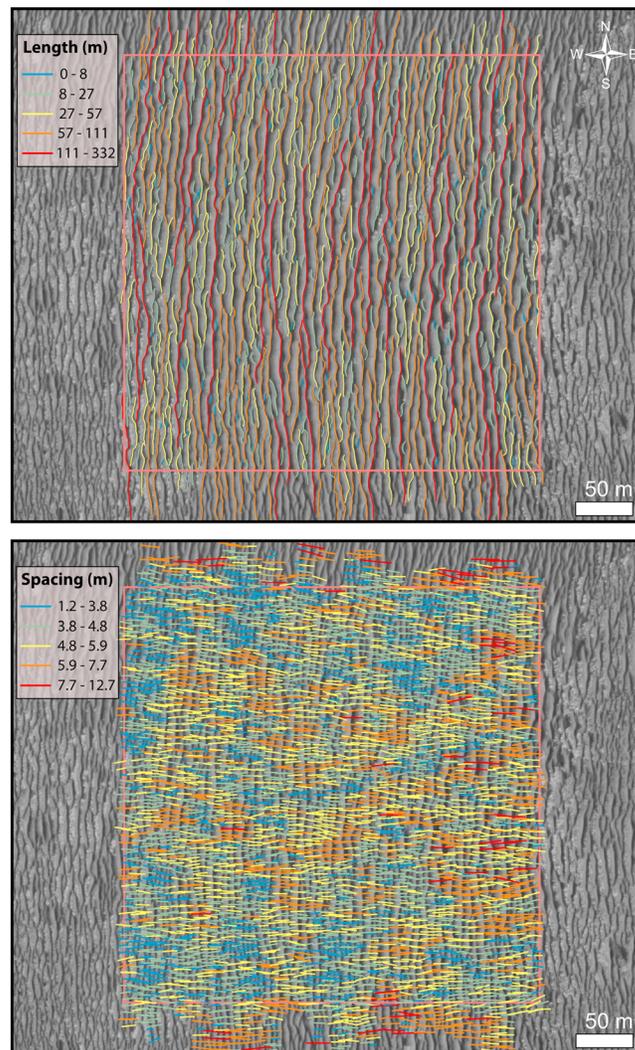
Figure 2. Example of the sampled bed form crestlines (length and wavelength), see Figure 5e for location (HiRISE image ESP_016644_1780).

3. Results

3.1. Bed Form Pattern Groups

3.1.1. Visual Inspection

We identified three main morphologic bed form populations in HiRISE imagery (Figures 5 and 6). Population 3 is confined inside craters and consists of NE-SW trending rectilinear bed forms that are superimposed upon the N-S trending bed forms of population 2 (Figures 5a–5d). These features can also be found in craters lacking TAR fields. Population 2 can be divided into two different subpopulations. Subpopulation 2a is composed of reticulate TARs, 0.1–1 m in height, and is confined to the interior of impact craters (Figure 5). They have a main N-S trend with secondary and, in some cases, tertiary crests oriented at right angles (Figures 5c and 5d). The bed forms observed by Opportunity in Victoria Crater [*Squyres et al.*, 2009] belong to this population. Subpopulation 2b consists of relatively shorter wavelength N-S trending megaripples (plains ripples), 0.1–0.4 m in height and are mainly located on the plain. These bed forms can be found in continuity with (Figure 5d) or stratigraphically below subpopulation 2a (Figure 5f). 2b ripple topography were probably important in triggering erosion on the underlying substrate as suggested for the Puna megaripples in Argentina [*de Silva et al.*,
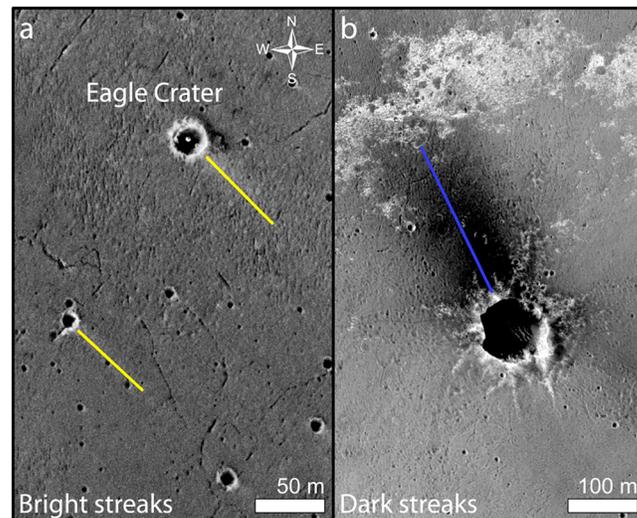
Figure 3. Mapped active wind streaks. (a) Bright streaks. (b) Dark wind streaks (HiRISE image ESP_021747_1780).
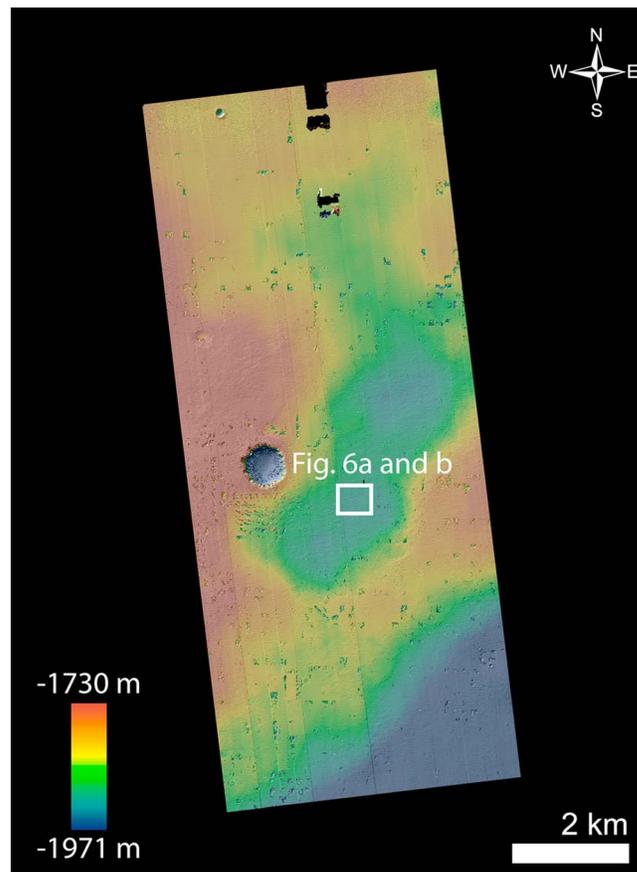
Figure 4. DTM derived from the HiRISE stereo couple ESP_022380_1780/ESP_021747_1780. We measured the bed form pop. One height in the area highlighted by the white rectangle which is not influenced by any of the errors that locally affect DTM quality.

2013] and highlighted by *Fenton et al.* [2015]. Much of Opportunity's traverse across the Meridiani plains was through subpopulation 2b bed forms. A good example is the Rub Al Khali panorama created from images acquired on sols 456 to 464 at the MER Opportunity site [*Squyres et al.*, 2006]. 2b megaripples are grouped in bands defining an additional orientation trending E-W, the population 1 (Figure 6). Population 1 is widespread in the landing ellipse (Figure 1a) and appears as a bright/dark banding on HiRISE images formed by ripple of different wavelengths (Figure 6a). Higher wavelength 2b ripples mark the different bands with the tallest (>0.30 m) being clearly visible in the DTM as elevated ridges (Figures 6b and 6c and supporting information Animation S1). The E-W trending ridges are locally deflected by eroded Noachian impact craters (Figure 6d) and show Y junction terminations (Figures 6a and 6b inset and Figure 6e), which are typical of aeolian bed forms [*Tsoar*, 1983, 2001; *Werner and Kocurek*, 1999].

3.1.2. Bed Form Pattern Measurements

In Figure 7a we show a rose diagram of the trend measurements for the bed form populations visually identified. Bed forms lying inside impact craters such as population 3 and subpopulation 2a, reticulate TARs, present a higher directional variability (Circular Standard Deviation (CSD) varying between 17 and 40° respectively, Table 2). Subpopulation 2b, plain ripples, shows the lowest trend variability with the measurements being tightly distributed around 2.4° (Table 2). Despite being mainly located on the plains, the bed form population 1 also presents a high CSD. A possible explanation is the effect of nearby crater topography, which locally deflects the main E-W trend (Figures 6d and 6e and Table 2).

In Figure 7b we show cumulative log probability plots of crestline wavelength and length distributions [*Beveridge et al.*, 2006; *Ewing et al.*, 2006, 2010]. With the
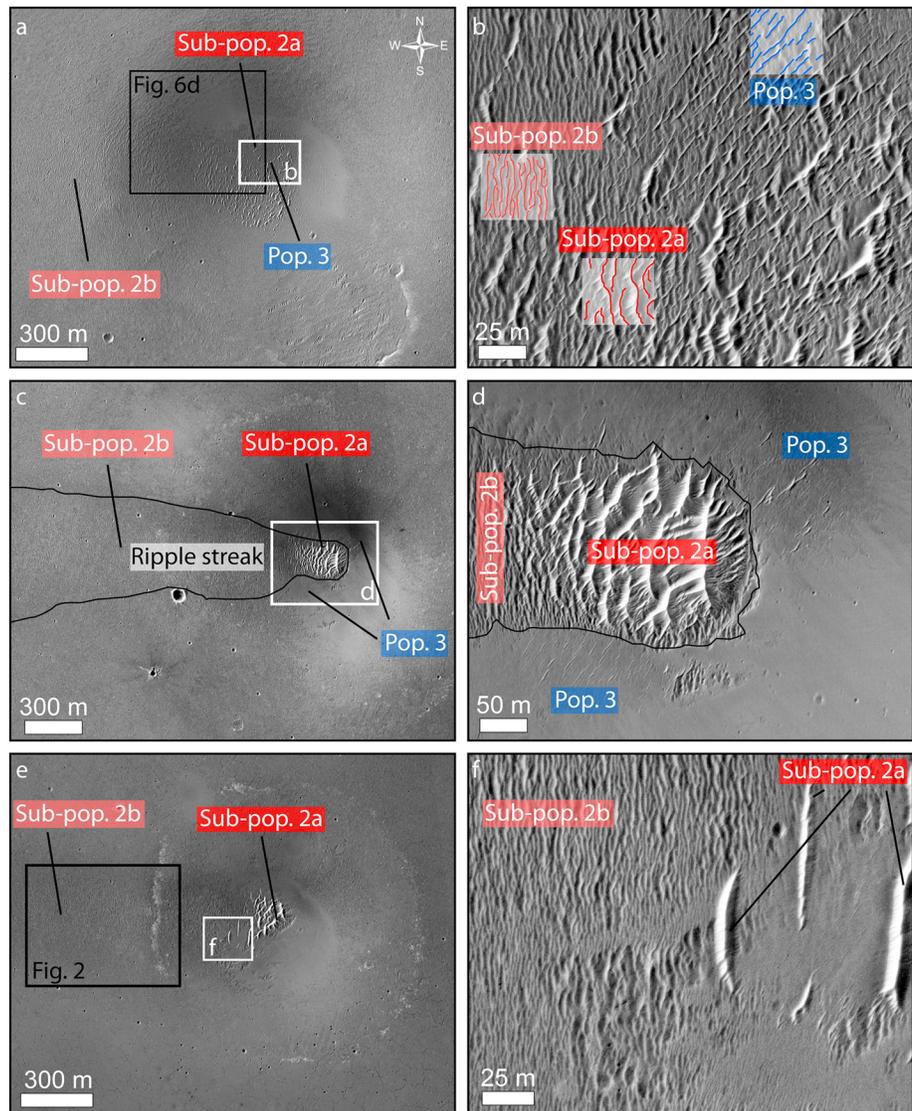
Figure 5. Bed form populations 3 and 2. (a) Location map for Figure 5b. (b) Complex pattern formed by the population 3 and by the subpopulations 2a (TARs) and 2b (plain ripples). (c) Location map for Figure 5d. (d) The subpopulations 2a and 2b can be found in continuity to form ripple streaks. (e) Location map for Figure 5f. (f) Superposition relationship between the subpopulations 2a and 2b (Figures 5a and 5b, HiRISE ESP_034986_1785 and Figures 5c–5f, HiRISE ESP_034274_1780).

exception of subpopulations 2a and 2b, which can occur together in the ripple streak (see section 3.2), each group is plotted as a separate population. In these plots a single population consists of a straight line and the median value is at the 50th percentile. The slope of the line correlates with the variability which is numerically related to the coefficient of variation (CV) [*Ewing et al.*, 2010]. CV values <0.5 indicate a high degree of homogeneity in the measurements [*Beveridge et al.*, 2006].

The plots of Figure 7b show that the bed form populations distinguished visually constitute distinct populations and that two different subclasses form population 2. Consistent with *Ewing et al.* [2006], wavelength measurements are the most useful parameters to distinguish different patterns (see the partial overlapping between populations 2 and 3 in the lognormal length distribution plot). With the exception of the entire population 2, the coefficient of variation for the wavelength measurements is relatively low (0.33–0.47) compared to the crest length measurements (0.73–1.26), meaning that spacing values are more homogeneous (Table 2). This result is in agreement with similar results for the Gran Desierto of Sonora in Mexico [*Beveridge et al.*, 2006].
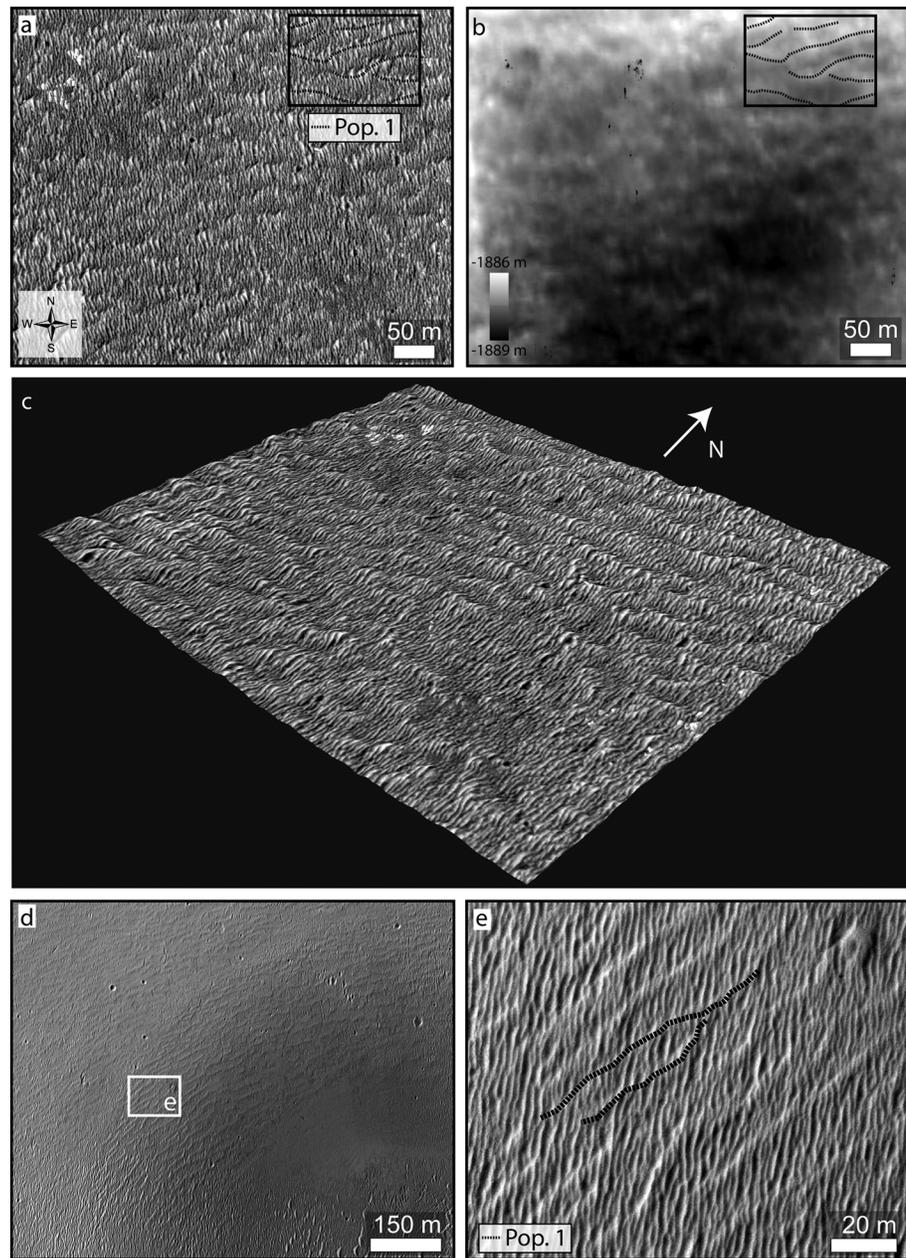
Figure 6. Bed form population 1. (a) HiRISE image showing the E-W spatial arrangement of the subpopulation 2b ripples. (b) Topographic expression of the population 1 ridges on HiRISE DTM. (c) Three-dimensional view of the bed form population 1 (vertical exaggeration 10X). (d, e) The population 1 trend is deflected by the rim of an ancient Noachian crater (Figure 6a, HiRISE ESP_021747_1780; Figure 6b, DTM derived from the HiRISE stereo couple ESP_022380_1780/ESP_021747_1780; Figure 6c, HiRISE ESP_021747_1780 draped over the DTM; and Figures 6d and 6e, HiRISE ESP_034986_1785).

In Figure 7b (top) we show the lognormal wavelength distribution for the three bed form populations. Bed form population 3 ranges in wavelength between 1 and 20 m with 95% of the measured values being less than 10 m. Population 3 wavelength plots as a straight line with no inflections meaning that the bed forms sampled in HiRISE data among the ellipse belong to a unique and distinct population. Bed form population 2 shows a clear inflection in the wavelength measurements that reflects the two subpopulations visually identified (secondary and tertiary bed forms are not considered in Figure 7). Population 1 shows the highest median values of wavelength and length measurements. Wavelength values are homogeneous,
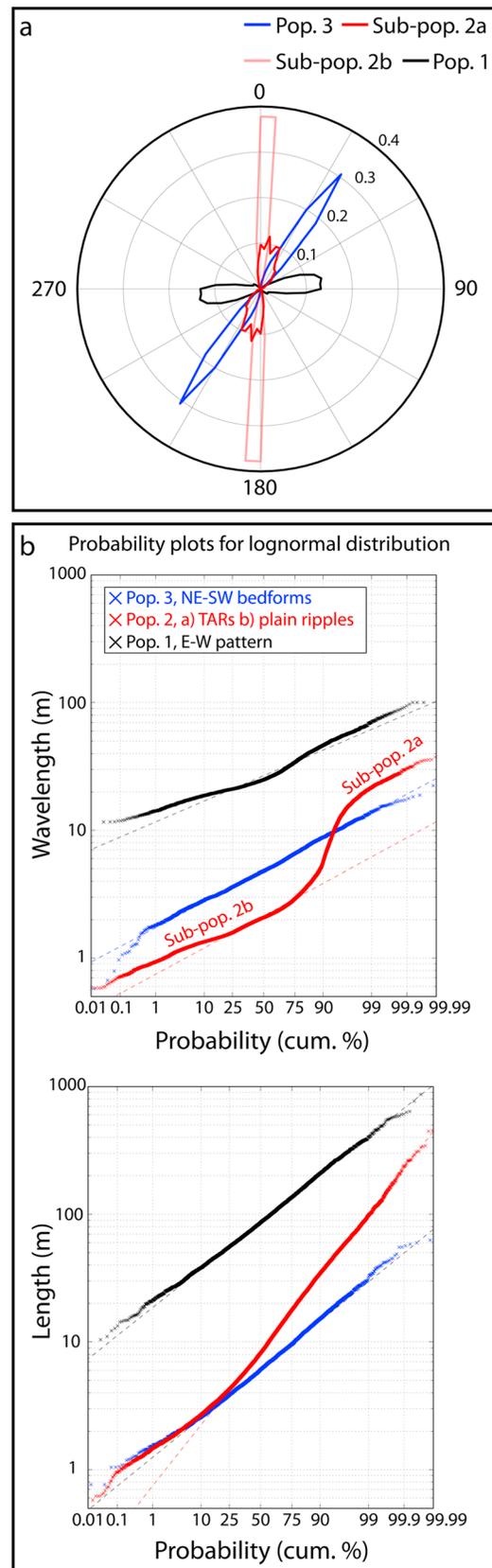
varying between 10 to 100 m with the median at 27.2 m (Table 2). An inflection is visible in the wavelength measurements at ~25 m. In Figure 7b (bottom) we show the lognormal length distributions. Length measurements for populations 2 and 3 are highly variable. Because topography is a well-known boundary condition that can influence bed form development [*Ewing and Kocurek*, 2010], population 3 length variability may be due to the different crater sizes where the bed forms evolved. For population 2, bed form length and defect terminations cannot always be clearly distinguished, especially in areas where bed forms are closely spaced (supporting information Figure S2), causing the high variability of the length measurements. Length measurements for population 1 span 2 orders of magnitude.

3.2. Ripple Streaks

Beside the complex arrangement of the distinct groups of bed forms indentified on HiRISE, we also noticed another important characteristic: the spatial distribution of the bed forms grouped in population 2 (TARs and plain ripples) are strongly topographically controlled. In particular, the plain ripples of subpopulation 2b tend to cluster in the wake zone of impact craters forming "megaripple tails" (ripple streaks) which extend downwind to the west (mode at 270°) (Figure 8). These features are widespread in the whole Meridiani region and in the landing site (Figures 8a and 8b) and have lower thermal inertia values relative to the surrounding plains which can indicate a higher concentration of fines [*Arvidson et al.*, 2011]. We investigated the spacing distribution of the bed forms forming the ripple streaks in one typical example (Figure 8c). Wavelength measurements decrease westward and change in the N-S direction too. Higher wavelength bed forms are located in the middle of the streaks, grading into smaller wavelength ripples toward the edges (Figure 8c). Ripple streaks are visible in the landing ellipse together with other types of wind streaks, the bright and dark wind streaks [*Thomas et al.*, 1981] (Figure 8b).

Figure 7. Statistical parameters for the bed form populations identified in the study area (a) Bed form crestlines length-weighted circular distributions. (b) Lognormal frequency plots of crestlines wavelength and length. Note the different trends and wavelengths of the three populations and the sharp discontinuity in the wavelength lognormal plot which denote the existence of two subpopulations (subpopulations 2a and 2b). The population 1 also shows an inflection which might indicate the presence of a second population of wavelength.

Table 2. Statistical Summary of Bed Form Pattern Measurements

| Population | N | Trend (°) | | | Wavelength (m) | | | | Length (m) | | | |
		Beform Type	Mean Azimuth	CSD	Mean	Median	SD	CV	Mean	Median	SD	CV
3	3897	TARs (?)	32.7	17	5.4	4.9	2.5	0.47	8	6.2	6.2	0.76
2	13198	TARs + plain ripples	4.8	22	3.2	2.5	2.7	0.82	22	14.5	26	1.16
2a	1618	TARs	17	40	15.0	13.5	7.1	0.47	36	22.4	45	1.26
2b	11580	Plain ripples	2.4	9.8	2.1	2	0.70	0.33	20	13.6	23	1.11
1	5341	(?)	85.3	33	29.1	27.2	11	0.37	109	87.7	79	0.73

3.3. Active Wind Streaks

In order to understand the direction of the present-day winds in the study area we mapped the location and orientation of the active wind streaks (Figures 3 and 8b). We group these features in two main categories, dark and bright streaks, following the classification of *Thomas et al.* [1981]. Bright depositional wind streaks consist of dust that accumulates in the lee of impact craters during major dust storm events. These features are transient and have been observed to change direction [*Sullivan et al.*, 2005; *Jerolmack et al.*, 2006]. Their orientation in the study area is toward the NW and the SE with two modes at ~120° and ~330° (see rose diagram in Figure 8b). Dark streaks can be erosional (type I) or depositional (type II) [*Thomas et al.*, 1981; *Vevereka et al.*, 1981], and their orientation is similar to the bright streaks with modes at ~120° and ~300° (Figure 8b). These orientations are consistent with the ones reported by other authors [*Jerolmack et al.*, 2006; *Fenton et al.*, 2015].
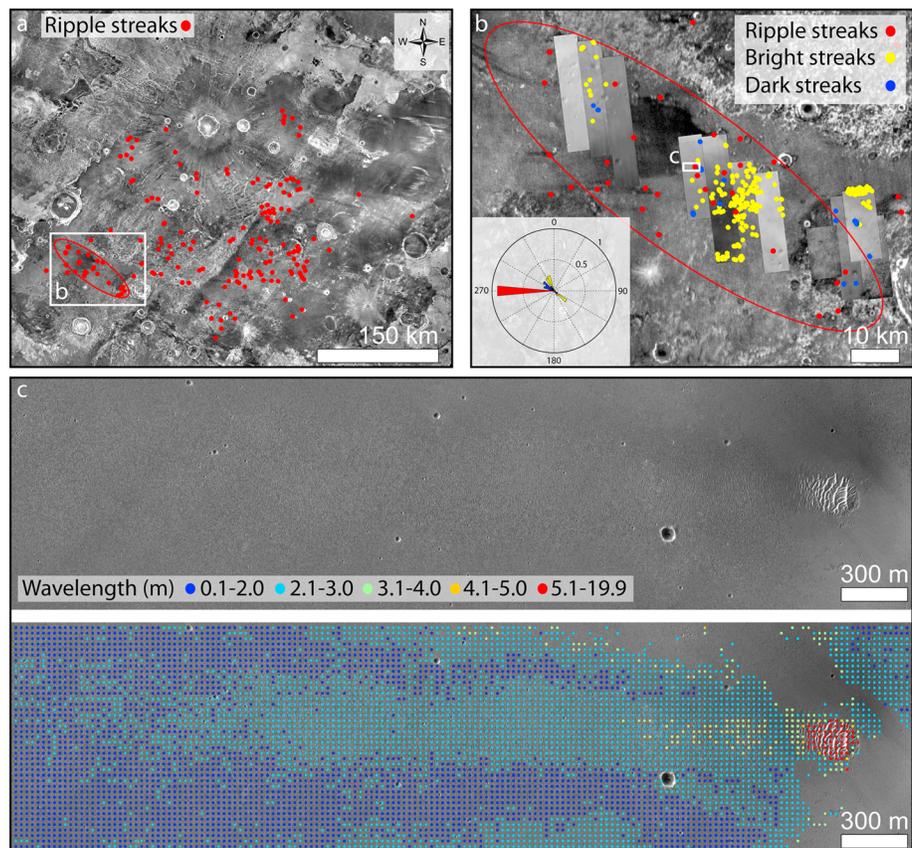
Figure 8. Wind and ripple streaks. (a) Ripple streak location in Meridiani Planum. (b) Ripple and wind streak location and orientation (rose diagram in inset) in the ESA ExoMars 2016 landing site. (c) Bed forms wavelength spatial distribution along a typical ripple streak, with the higher wavelength bed forms located in the middle of the streak and with a longitudinal variation possibly influenced by the upwind crater topography (Figures 8a and 8b, THEMIS IR nighttime mosaic and Figure 8c, HiRISE ESP_034274_1780).
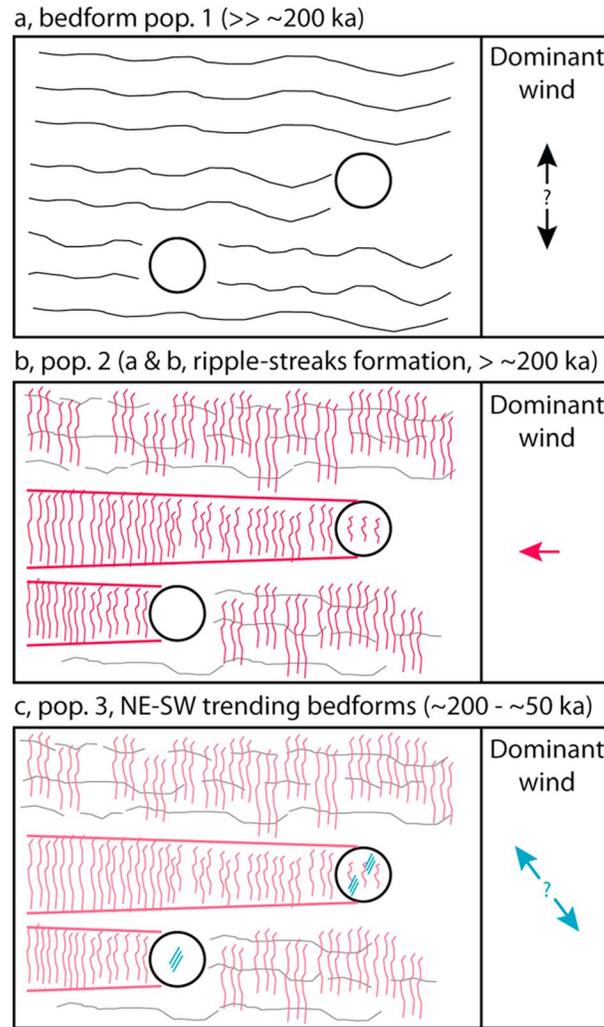
Figure 9. Schematic drawing showing the interpreted evolution of the complex pattern in Meridiani Planum. Age constraints taken from *Fenton et al.* [2015].

4. Discussion

4.1. Geomorphic Backstripping and Wind Regimes

Collectively, our results show that the ExoMars 2016 landing ellipse in Meridiani Planum has been subject to diverse winds that have generated a complex bed form pattern. The statistical analysis of multiple bed form populations supports this interpretation. The development of a complex pattern implies that each bed form generation is indicative of a distinct constructional event linked to specific boundary conditions (wind regime, sediment supply, and sediment availability in the terminology of *Kocurek and Lancaster* [1999]). In particular, the development of a complex pattern implies a temporal shift in the main wind directions that occurs at a higher rate than the construction period of the slowest moving bed forms [*Kocurek and Ewing*, 2005].

We identified three distinct episodes of aeolian construction in the study area (Figure 9). All of them are likely to have occurred during the Amazonian/Late Amazonian epoch [*Fenton et al.*, 2015]. The nature of the population 1 is more enigmatic, and we propose two mechanisms for the formation of these features: (1) reworking of a relict pattern and (2) a longitudinal "ribbon pattern" [*Allen*, 1968, 1982] formed by the 2b ripple population. Several indicators support the first mechanism which implies that similar to terrestrial counterparts [e.g., *Beveridge et al.*, 2006, Figure 4], the elevated E-W trend represents a relict bed form pattern subsequently reworked by the bed forms of population 2b (Figures 9a and 9b). On a smaller scale, a similar bed form arrangement has been directly observed by Opportunity in the vicinity of Eagle Crater (e.g., N4°E ripple pattern described by *Sullivan et al.* [2005]) (Figure 10a) and on its traverse south toward Victoria Crater (Figure 10b). *Golombek et al.* [2010] argued that the N-S trending plain ripples (population 2b) formed before the unnamed 0.84 km in diameter impact crater dated 200 ka. This means that population 1 should be ≫~200 ka. Population 1 wavelengths (29 m on average, Table 2) seem to be too small for a paleoerg formed by simple dunes (50–500 m) [*Lancaster*, 1995]. Instead, the measured wavelengths are more consistent with Martian TAR and large terrestrial megaripple values [*Balme et al.*, 2008; *Milana*, 2009; *de Silva et al.*, 2013; *Geissler*, 2014]. The high length variability might reflect the breakup of the crestlines that have been severely reworked while the inflection in the spacing distribution can indicate different subpopulations. However, due to the highly degraded state of population 1 pattern, it is impossible to segregate visually distinct subpopulations as we did for population 2. The wavelength variations characterizing the overlapping 2b ripple trains, which directly source from population 1, can be indicative of grain size bimodality [*Greeley and Iversen*, 1985]. Grain size bimodality has also been directly observed by Opportunity in Meridiani [*Sullivan et al.*, 2005; *Squyres et al.*, 2006; *Weitz et al.*, 2006] and is thought to be common on TARs and megaripples in Meridiani and elsewhere on Mars [*Arvidson et al.*, 2006; *Minitti et al.*, 2013].

Figure 10. Opportunity view of the plain ripples in Meridiani Planum. (a) Navcam image of the plain ripples in the vicinity of Eagle Crater with the two orientations described by *Sullivan et al.* [2005]. (b) Left Panoramic Camera Image acquired on sol 385 of the plain ripples (trend N-S) which are locally reworked by oblique winds (subpopulation 2b).

This suggests that population 1 may represents one of these two classes of bed forms. On Earth, ripples of similar size develop during extremely strong wind events [*Milana*, 2009], suggesting that such strong winds should have been common on Mars, perhaps during a high-obliquity axis period when winds were predicted to be stronger [*Haberle et al.*, 2003; *Geissler*, 2014]. Their widespread occurrence in the landing ellipse also suggests an extensive source area. Assuming that population 1 bed forms are transverse and not oblique or longitudinal, their E-W trend indicates formative winds coming from the north or from the south (Figure 9a). These wind directions do not match the present-day winds deduced from the active wind streak orientations. Population 1 bed forms postdate the Burns Formation where northward and southward dipping cross beds have been imaged by Opportunity [*Hayes et al.*, 2011]. This observation suggests that such winds were common in the past and provides additional evidence in support of the relict pattern hypothesis. An alternative explanation is that the E-W trend represents a ribbon pattern [*Bagnold*, 1954; *Allen*, 1968, 1982] (Figure 11). Sand ribbons or sand streams [*Simons and Ericksen*, 1953] have been mainly reported from subaqueous environments as "longitudinal ripples" [*Van Straaten*, 1951; *Tucholke*, 1982]. Detailed studies of desert sand ribbons are, to our knowledge, scarce. *Bagnold* [1954] reported sand ribbons features developing during a storm in the Libyan Desert while *Simons and Ericksen*, 1953 and subsequently *Rinker et al.* [1991] described ribbons forming in coarse/medium sand south of the city of Pisco in Perù (Figure 11a). The author personally observed sand ribbons over the stoss side of barchanoid dunes at Dillon Beach in California (USA) (Figures 11b and 11c). Ribbons features represent a mode of self-organization that is still poorly understood. *Bagnold* [1954] argued that small-scale rotatory flows caused by the change in

the roughness at the flow/bed interface can generate longitudinal stripe of sand. Thus, ribbons' occurrence seems to be related to strong unidirectional winds acting on bimodal sand bed. This would change our evolutionary scenario with population 1 pattern forming together with population 2b under the influence of the same strong easterlies >~200 ka ago (Figure 9b). However, ribbon features on Earth form more organized patterns (Figure 11a) compared to the one we observe in the study area, making this hypothesis less likely. The interpretative ambiguity about the nature of population 1 can only be solved by future in situ studies, aimed to better comprehend the reworking of older structures by aeolian activity as well as the processes that control the formation of sand ribbons on Earth.

Population 2 is the second episode of aeolian construction represented by the emplacement of the plain ripples (subpopulation 2b), the accumulation of TARs inside impact craters (subpopulation 2a) and the formation of the ripple streaks (see section 4.2) ~200 ka ago (Figure 9b). Subpopulation 2b bed forms may have evolved differently from the intracrater TARs, with the latter being activated more recently and
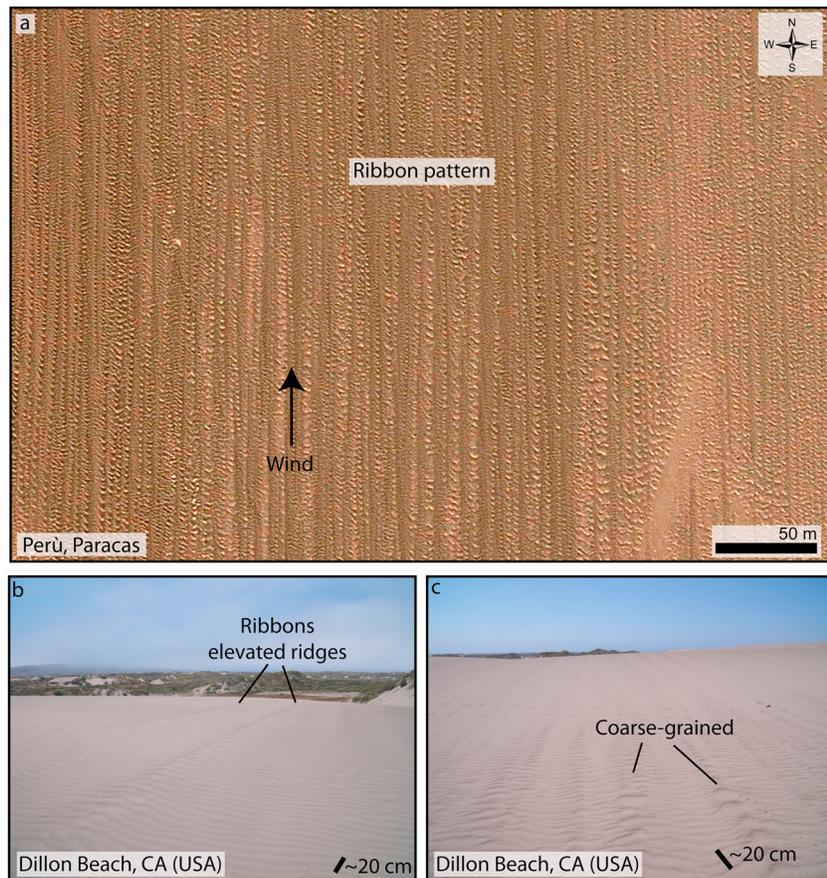
Figure 11. Ribbon pattern. (a) Paracas Peninsula (Perù), field of transverse megaripples forming a more organized longitudinal ribbon pattern, image extracted from Google Earth centered at 13°51′45.07″S 76°14′31.12″O. (b, c) Ribbon pattern over the stoss side of aeolian barchanoid dunes at Dillon Beach, CA (USA), 38°14′29.71″N 122°57′40.26″O. Photos taken by the author.

subsequently migrating over the slower-moving plain ripples (Figure 5f) [*Fenton et al.*, 2015]. However, as also discussed by *Fenton et al.* [2015], the ambiguity of the superposition relationship between TARs and plain ripples prevents us to clearly separate the two populations, meaning that the sketch showed in Figure 9b is probably oversimplified. The main N-S trend of population 2 bed forms (both TARs and plain ripples) can be coupled with in situ Opportunity observations of the ripple foresets [*Golombek et al.*, 2010] to derive the formative wind direction which is from the east. The higher complexity of the intracrater TARs can be explained by considering the influence of crater topography. This can probably explain their "ladderback" [*Reddering*, 1987; *Ramsay et al.*, 1989] appearance without involving a progressive build up from individual "deltoid" components [*Geissler*, 2014]. The dominance of winds from the east implies a dramatic shift in the main wind direction (90° or 270°). Such wind variation has been attributed to planetary obliquity changes, a theory that needs to be confirmed by new model simulations [*Fenton and Richardson*, 2001; *Arvidson et al.*, 2011].

Population 3 bed forms represent the most recent episode of aeolian construction recognized in the landing ellipse. *Fenton et al.* [2015] argued that bed form activity should postdate the impact of the secondaries from the ~200 ka unnamed crater dated by *Golombek et al.* [2010]. On the other hand, the ~50 ka Resolution crater cluster seem to have impacted after the latest phase of ripple migration [*Golombek et al.*, 2010]. This means that population 3 emplacement occurred between ~50 ka and ~200 ka (Figure 9c). The active large dark dunes [*Chojnacki et al.*, 2011, 2014; *Silvestro et al.*, 2011] are surely younger and represent a separate episode of aeolian construction [*Fenton et al.*, 2015]. However, these dunes are not treated in this work because they are not present in the 2016 ExoMars landing area. Population 3 location is limited to the interior of impact craters, suggesting that topography strongly influences their formation. This situation is similar to
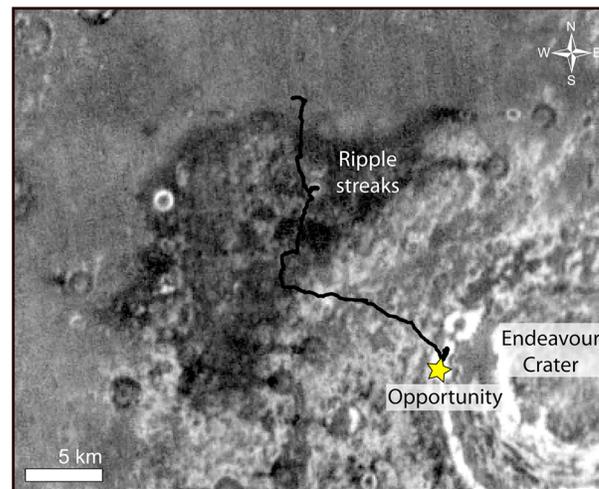
Figure 12. Opportunity path across the ripple streaks in Meridiani Planum (THEMIS IR nighttime mosaic).

the present-day aeolian sediment state [*Kocurek and Ewing*, 2012], where dunes are locally sourced [*Tirsch et al.*, 2011] and kept active by strong, topographically controlled winds [*Cardinale et al.*, 2012; *Silvestro et al.*, 2012]. Assuming a transverse nature for these features, their trend indicates that they were formed by winds blowing from the NW or the SE. Both directions are in agreement with the present-day winds deduced from the bright and dark active wind streak orientations. However, population 3 bed forms are most likely TARs which are not active in the current wind regime [*Reiss et al.*, 2004; *Kerber and Head*, 2012]. This suggests that the dominant winds that have generated population 3 were stronger than today and did not switch in direction since the formation of the active wind streaks. A combination of weaker easterly wind with more prominent NW/SE flows is also in accord with the observed bed form orientations as suggested by *Fenton et al.* [2015].

4.2. Ripple Streaks

Ripple streaks can be classified as a new type of wind streak for several reasons. Unlike the streaks described in previous works [e.g., *Sagan et al.*, 1972; *Thomas et al.*, 1981], ripple streaks are inactive in the present-day atmospheric setting and do not source from an intracrater deposit. Their association with impact structures clearly suggests that crater topography played a key role in generating local wind conditions favorable for bed form development, as showed in laboratory experiments [*Tyler*, 1979; *Greeley and Iversen*, 1985]. Crater topography is hypothesized to interact with the wind flow in two ways: (1) by causing blocking and "wind shadowing" in atmospheric stable conditions (similar to the formation mechanism for bright dust depositional streaks) and (2) by increasing surface stress during periods of atmospheric instability (a condition thought to be important for the formation of dark erosional streaks) [*Vevereka et al.*, 1981]. Taking into account the linear dependence between wind velocity, granulometry, and ripple wavelength described from laboratory studies [*Seppälä and Lindé*, 1978; *Andreotti et al.*, 2006], the observed wavelength distribution can be related to the higher wind speed in the lee of the crater. Alternatively, grain size segregation can control the ripple spacing, with the coarser fraction lagging closer to the impact structure causing higher wavelength ripples to form near the crater and smaller wavelength ripples to develop further west. These two factors can help to explain both E-W and N-S wavelength variations, but their relative contributions can only be assessed by using mesoscale/microscale wind models [*Rafkin et al.*, 2001; *Smyth et al.*, 2012] and detailed in situ investigations.

The westward direction and the regional occurrence of the ripple streaks give further hints on the regional easterlies that emplaced the population 2 bed forms >~200 ka ago. These winds differ from the present-day wind directions deduced from the active wind streak orientations.

4.3. Implications for ExoMars 2016 and Opportunity Missions

The ExoMars 2016 Entry descent and landing Demonstrator Module (EDM) that is targeted to land in Meridiani Planum in 2016 will carry on board a meteorological station (Dust Characterization, Risk Assessment, and Environment Analyser on the Martian Surface (DREAMS)), which consists of the following subsystems: MarsTEM (Thermometer), DREAMS-P (Pressure sensor), DREAMS-H (Humidity sensor), MetWind (2-D Wind sensor), MicroARES (electrical field sensor), solar irradiance sensor, a Central Electronic Unit, and a battery [*Bettanini et al.*, 2014; *Esposito et al.*, 2014a, 2014b].

Based on the results of this work, we now know that the landing ellipse presents a complex aeolian environment. The bed form populations described in this work are currently inactive. However, the widespread presence of

active wind streaks (Figure 8b) together with other evidence of aeolian activity inside and close to the landing ellipse [*Geissler et al.*, 2010; *Chojnacki et al.*, 2011, 2014; *Silvestro et al.*, 2011], suggest that sand saltation and dust lifting are common in the landing area. Therefore, DREAMS might have the opportunity to operate in an active aeolian environment maximizing its scientific return. Further measurements of wind strength and direction at the landing site will be useful to better characterize the NW-SE winds that currently drive the bright and dark streak activity.

The inactive ripple streaks are of interest because they provide precious paleo-environmental information. Because the present-day flow pattern may still be influenced by the craters topography, the DREAMS package might be able to characterize the atmospheric conditions that can promote bed form development (e.g., enhanced stress on the surface). These data can be critical to test high-resolution atmospheric simulations and regional mesoscale models [*Rafkin et al.*, 2001; *Smyth et al.*, 2012]. Furthermore, the rover Opportunity crossed the ripple streaks during sols 384 to 2320 (Figure 12). Rover images can shed light on the streak formation mechanism by comparing the morphology and granulometry of the megaripples within and outside ripple streak zones.

5. Summary and Conclusion

We show that a complex history of sediment transport led to the development of a multigenerational bed form pattern within the landing ellipse of the ExoMars 2016 mission. Bed form morphologies reflect a change in the aeolian sediment state from strong regionally blowing winds and widespread source areas to local topographically controlled wind events and more localized sources.

The most likely evolutionary scenario involves three main episodes of aeolian bed form constructions (from the older to the younger): (1) a paleo bed form pattern trending E-W, population 1, has been emplaced by winds coming from the N or from the S; (2) a directional shift of 90° (or 270°) of the wind regime lead to the accumulation of the TARs inside craters and to the reworking of population 1 by the N-S trending plain ripples (subpopulations 2a and 2b). The same winds promoted the formation of bed forms in the wake of impact craters to form a newly recognized type of wind streak, the ripple streaks. The regional occurrence of these features indicates that winds from the east were not limited to the study area, but were regionally blowing. (3) A further change in the wind direction formed the population 3 bed forms inside impact craters. Alternatively, the population 1 pattern might represent a ribbon pattern, which formed together with population 2b megaripples under the influence of the same dominant easterlies.

With the exception of the population 3 pattern, the direction of the winds responsible for the emplacement of the aeolian features described in this work differ from the present-day wind directions. This provides further evidence on the wind directional variability that characterized the geological history of Meridiani Planum.

Future measurements from the ExoMars 2016 DREAMS package, combined with Opportunity data can help to better decipher nature of the population 1 and the wind regime in Meridiani Planum, providing insights on regional wind changes and on ripple streaks formation mechanism.

References

Allen, J. R. L. (1968), *Current Ripples: Their Relation to Patterns of Water and Sediment Motion*, North-Holland Pub. Co, Amsterdam.
Allen, J. R. L. (1982), *Sedimentary Structures, Their Character and Physical Basis, Volume 2*, Elsevier Science, New York.
Andreotti, B., P. Claudin, and O. Pouliquen (2006), Aeolian sand ripples: Experimental study of fully developed states, *Phys. Rev. Lett.*, *96*(2), 1–4, doi:10.1103/PhysRevLett.96.028001.
Arvidson, R. E., et al. (2004), Localization and physical property experiments conducted by Opportunity at Meridiani Planum, *Science*, *306*(5702), 1730–1733, doi:10.1126/science.1104211.
Arvidson, R. E., et al. (2006), Nature and origin of the hematite-bearing plains of Terra Meridiani based on analyses of orbital and Mars Exploration rover data sets, *J. Geophys. Res.*, *111*, E12S08, doi:10.1029/2006JE002728.
Arvidson, R. E., et al. (2011), Opportunity Mars Rover mission: Overview and selected results from Purgatory ripple to traverses to Endeavour crater, *J. Geophys. Res.*, *116*, E00F15, doi:10.1029/2010JE003746.
Bagnold, R. A. (1954), *The Physics of Blown Sand and Desert Dunes*, 2nd ed., Dover Publ., Inc., Mineola, New York.
Balme, M., D. C. Berman, M. C. Bourke, and J. R. Zimbelman (2008), Transverse Aeolian Ridges (TARs) on Mars, *Geomorphology*, *101*(4), 703–720, doi:10.1016/j.geomorph.2008.03.011.
Bettanini, C., F. Esposito, S. Debei, C. Molfese, I. A. Rodríguez, G. Colombatti, and A. Harri (2014), The DREAMS experiment on the ExoMars 2016 mission for the study of Martian environment during the dust storm season, in *Proceedings of IEEE Metrology for Aerospace (MetroAeroSpace)*, pp. 167–173.

Beveridge, C., G. Kocurek, R. C. Ewing, N. Lancaster, P. Morthekai, A. K. Singhvi, and S. A. Mahan (2006), Development of spatially diverse and complex dune-field patterns: Gran Desierto Dune Field, Sonora, Mexico, *Sedimentology*, *53*(6), 1391–1409, doi:10.1111/j.1365-3091.2006.00814.x.

Bourke, M. C., N. Lancaster, L. K. Fenton, E. J. R. Parteli, J. R. Zimbelman, and J. Radebaugh (2010), Extraterrestrial dunes: An introduction to the special issue on planetary dune systems, *Geomorphology*, *121*(1–2), 1–14, doi:10.1016/j.geomorph.2010.04.007.

Bridges, N., P. Geissler, S. Silvestro, and M. Banks (2013), Bedform migration on Mars: Current results and future plans, *Aeolian Res.*, *9*, 133–151, doi:10.1016/j.aeolia.2013.02.004.

Cardinale, M., G. Komatsu, S. Silvestro, and D. Tirsch (2012), The influence of local topography for wind direction on Mars: Two examples of dune fields in crater basins, *Earth Surf. Processes Landforms*, *37*(13), 1437–1443, doi:10.1002/esp.3289.

Chojnacki, M., D. M. Burr, J. E. Moersch, and T. I. Michaels (2011), Orbital observations of contemporary dune activity in Endeavor crater, Meridiani Planum, Mars, *J. Geophys. Res.*, *116*, E00F19, doi:10.1029/2010JE003675.

Chojnacki, M., J. R. Johnson, J. E. Moersch, L. K. Fenton, T. I. Michaels, and J. F. Bell (2014), Persistent aeolian activity at Endeavour crater, Meridiani Planum, Mars: New observations from orbit and the surface, *Icarus*, doi:10.1016/j.icarus.2014.04.044.

Christensen, P. R., et al. (2004), The Thermal Emission Imaging System (THEMIS) for the Mars 2001 Odyssey Mission, *Space Sci. Rev.*, *110*, 85–130.

De Silva, S. L., M. G. Spagnuolo, N. T. Bridges, and J. R. Zimbelman (2013), Gravel-mantled megaripples of the Argentinean Puna: A model for their origin and growth with implications for Mars, *Geol. Soc. Am. Bull.*, *125*(11–12), 1912–1929, doi:10.1130/B30916.1.

Derickson, D., G. Kocurek, R. C. Ewing, and C. S. Bristow (2008), Origin of a complex and spatially diverse dune-field pattern, Algodones, southeastern California, *Geomorphology*, *99*(1–4), 186–204, doi:10.1016/j.geomorph.2007.10.016.

Esposito, F., C. I. Popa, G. Di Achille, C. Molfese, F. Cozzolino, L. Marty, K. Taj Eddine, and G. G. Ori (2014a), Field test campaign in the Morocco Desert as analog for the DREAMS experiment on board ExoMars 2016 Mission, in *45th Lunar and Planetary Science Conference*, p. 2411.

Esposito, F., et al. (2014b), The DREAMS experiment on the ExoMars 2016 Mission for the study of Martian environment during the dust storm season, in *Eight International Conference on Mars*, p. 1246.

Ewing, R. C., and G. Kocurek (2010), Aeolian dune-field pattern boundary conditions, *Geomorphology*, *114*(3), 175–187, doi:10.1016/j.geomorph.2009.06.015.

Ewing, R. C., G. Kocurek, and L. W. Lake (2006), Pattern analysis of dune-field parameters, *Earth Surf. Processes Landforms*, *31*(9), 1176–1191, doi:10.1002/esp.1312.

Ewing, R. C., A.-P. B. Peyret, G. Kocurek, and M. Bourke (2010), Dune field pattern formation and recent transporting winds in the Olympia Undae Dune Field, north polar region of Mars, *J. Geophys. Res.*, *115*, E08005, doi:10.1029/2009JE003526.

Fenton, L. K., and M. I. Richardson (2001), Martian surface winds: Insensitivity to orbital changes and implications for aeolian processes, *J. Geophys. Res.*, *106*(E12), 32,885–32,902, doi:10.1029/2000JE001407.

Fenton, L. K., T. I. Michaels, and M. Chojnacki (2015), Late Amazonian aeolian features, gradation, wind regimes, and Sediment State in the Vicinity of the Mars Exploration Rover Opportunity, Meridiani Planum, Mars, *Aeolian Res.*, *16*(2015), 75–99, doi:10.1016/j.aeolia.2014.11.004.

Geissler, P. E. (2014), The birth and death of transverse aeolian ridges on Mars, *J. Geophys. Res. Planets*, *119*, 2583–2599, doi:10.1002/2014JE004633.

Geissler, P. E., R. Sullivan, M. Golombek, J. R. Johnson, K. Herkenhoff, N. Bridges, A. Vaughan, J. Maki, T. Parker, and J. Bell (2010), Gone with the wind: Eolian erasure of the Mars Rover tracks, *J. Geophys. Res.*, *115*, E00F11, doi:10.1029/2010JE003674.

Geissler, P. E., N. W. Stantzos, N. T. Bridges, M. C. Bourke, S. Silvestro, and L. K. Fenton (2013), Shifting sands on Mars: Insights from tropical intra-crater dunes, *Earth Surf. Processes Landforms*, *38*(4), 407–412, doi:10.1002/esp.3331.

Golombek, M., K. Robinson, A. Mcewen, N. Bridges, B. Ivanov, L. Tornabene, and R. Sullivan (2010), Constraints on ripple migration at Meridiani Planum from Opportunity and HiRISE observations of fresh craters, *J. Geophys. Res.*, *115*, E00F08, doi:10.1029/2010JE003628.

Golombek, M. P., et al. (2006), Erosion rates at the Mars Exploration Rover landing sites and long-term climate change on Mars, *J. Geophys. Res.*, *111*, E12S10, doi:10.1029/2006JE002754.

Greeley, R., and J. Iversen (1985), *Wind as a Geological Process On Earth, Mars, Venus and Titan*, Cambridge Univ. Press, Cambridge.

Grotzinger, J. P., et al. (2005), Stratigraphy and sedimentology of a dry to wet eolian depositional system, Burns formation, Meridiani Planum, Mars, *Earth Planet. Sci. Lett.*, *240*, doi:10.1016/j.epsl.2005.09.039.

Haberle, R. M., J. R. Murphy, and J. Schaeffer (2003), Orbital change experiments with a Mars general circulation model, *Icarus*, *161*, 66–89, doi:10.1016/S0019-1035(02)00017-9.

Hayes, A. G., J. P. Grotzinger, L. A. Edgar, S. W. Squyres, W. A. Watters, and J. Sohl-Dickstein (2011), Reconstruction of eolian bed forms and paleocurrents from cross-bedded strata at Victoria Crater, Meridiani Planum, Mars, *J. Geophys. Res.*, *116*, E00F21, doi:10.1029/2010JE003688.

Jakosky, B. M., and R. J. Phillips (2001), Mars' volatile and climate history, *Nature*, *412*(July), 237–244.

Jerolmack, D. J., D. Mohrig, J. P. Grotzinger, D. A. Fike, and W. A. Watters (2006), Spatial grain size sorting in eolian ripples and estimation of wind conditions on planetary surfaces: Application to Meridiani Planum, Mars, *J. Geophys. Res.*, *111*, 1–14, doi:10.1029/2005JE002544.

Kerber, L., and J. W. Head (2012), A progression of induration in Medusae Fossae Formation transverse aeolian ridges: Evidence for ancient aeolian bedforms and extensive reworking, *Earth Surf. Processes Landforms*, *37*(4), 422–433, doi:10.1002/esp.2259.

Kirk, R. L., E. Howington-Kraus, B. Redding, D. Galuszka, T. M. Hare, B. A. Archinal, L. A. Soderblom, and J. M. Barrett (2003), High-resolution topomapping of candidate MER landing sites with Mars Orbiter Camera narrow-angle images, *J. Geophys. Res.*, *108*(E12), 8088, doi:10.1029/2003JE002131.

Kocurek, G., and R. C. Ewing (2005), Aeolian dune field self-organization—Implications for the formation of simple versus complex dune-field patterns, *Geomorphology*, *72*(1–4), 94–105, doi:10.1016/j.geomorph.2005.05.005.

Kocurek, G., and R. C. Ewing (2012), Source-to-sink: An Earth/Mars comparison of boundary conditions for eolian dune systems, in *Sedimentary Geology Mars*, edited by J. P. Grotzinger and R. E. Milliken, *SEPM Spec. Publ.*, *102*, 151–168, doi:10.2110/pec.12.102.0151.

Kocurek, G., and N. Lancaster (1999), Aeolian system sediment state: Theory and Mojave Desert Kelso dune field example, *Sedimentology*, *46*(3), 505–515.

Lancaster, N. (1995), *Geomorphology of Desert Dunes*, Routledge, New York.

McEwen, A. S., et al. (2007), Mars Reconnaissance Orbiter's High Resolution Imaging Science Experiment (HiRISE), *J. Geophys. Res.*, *112*, E05S02, doi:10.1029/2005JE002605.

McLennan, S. M., et al. (2005), Provenance and diagenesis of the evaporite-bearing Burns formation, Meridiani Planum, Mars, *Earth Planet. Sci. Lett.*, *240*, 95–121, doi:10.1016/j.epsl.2005.09.041.

Milana, J. P. (2009), Largest wind ripples on Earth?, *Geology*, *37*(4), 343–346, doi:10.1130/G25382A.1.

Minitti, M. E., et al. (2013), MAHLI at the Rocknest sand shadow: Science and science-enabling activities, *J. Geophys. Res. Planets*, *118*, 2338–2360, doi:10.1002/2013JE004426.

Moratto, S. Z. M., M. J. Broxton, R. A. Beyer, M. Lundy, and K. Husmann (2010), Ames Stereo Pipeline, NASA's Open Source Automated Stereogrammetry, in *41st Lunar and Planetary Science Conference*, p. 2364.

Okubo, C. H. (2010), Structural geology of Amazonian-aged layered sedimentary deposits in southwest Candor Chasma, Mars, *Icarus*, *207*(1), 210–225, doi:10.1016/j.icarus.2009.11.012.

Rafkin, S. C. R., R. M. Haberle, and T. I. Michaels (2001), The Mars Regional Atmospheric Modeling System: Model description and selected simulations, *Icarus*, *151*(2), 228–256, doi:10.1006/icar.2001.6605.

Ramsay, P. J., J. A. G. Cooper, C. I. Wright, and T. R. Mason (1989), The occurrence and formation of ladderback ripples in subtidal, shallow-marine sands, Zululand, South Africa, *Mar. Geol.*, *86*(2–3), 229–235, doi:10.1016/0025-3227(89)90051-0.

Reddering, J. S. V. (1987), Subtidal occurrences of ladder-back ripples: Their significance in palaeo-environmental reconstruction, *Sedimentology*, *34*, 253–257.

Reiss, D., S. van Gasselt, G. Neukum, and R. Jaumann (2004), Absolute dune ages and implications for the time of formation of gullies in Nirgal Vallis, Mars, *J. Geophys. Res.*, *109*, E06007, doi:10.1029/2004JE002251.

Rinker, J. N., C. S. Breed, J. F. McCauley, and P. A. Corl (1991), Remote sensing field guide in Desert, *Tech. Rep.* 1985–1991.

Sagan, C., J. Veverka, P. Fox, R. Dubisch, J. Lederberg, E. Levinthal, L. Quam, and R. Tucker (1972), Variable features on Mars: Preliminary mariner 9 television results, *Icarus*, *372*(17), 346–372.

Seppälä, M., and K. Lindé (1978), Wind tunnel studies of ripple formation, *Geogr. Ann. Phys. Geogr.*, *60*, 29–42.

Silvestro, S., D. A. Vaz, L. K. Fenton, and P. E. Geissler (2011), Active aeolian processes on Mars: A regional study in Arabia and Meridiani Terrae, *Geophys. Res. Lett.*, *38*, L20201, doi:10.1029/2011GL048955.

Silvestro, S., L. K. Fenton, T. I. Michaels, A. Valdez, and G. G. Ori (2012), Interpretation of the complex dune morphology on Mars: Dune activity, modelling and a terrestrial analogue, *Earth Surf. Processes Landforms*, *37*(13), 1424–1436, doi:10.1002/esp.3286.

Simons, F. S., and G. E. Ericksen (1953), Some desert features of northwest central Peru, *Bol. la Soc. Geol. del Perù*, *26*, 229–246.

Smyth, T. A. G., D. W. T. Jackson, and J. A. G. Cooper (2012), High resolution measured and modelled three-dimensional airflow over a coastal bowl blowout, *Geomorphology*, *177–178*, 62–73, doi:10.1016/j.geomorph.2012.07.014.

Squyres, S. W., et al. (2006), Overview of the Opportunity Mars Exploration Rover Mission to Meridiani Planum: Eagle Crater to Purgatory Ripple, *J. Geophys. Res.*, *111*, E12S12, doi:10.1029/2006JE002771.

Squyres, S. W., et al. (2009), Exploration of Victoria crater by the Mars rover Opportunity, *Science*, *324*(5930), 1058–1061, doi:10.1126/science.1170355.

Sullivan, R., et al. (2005), Aeolian processes at the Mars Exploration Rover Meridiani Planum landing site, *Nature*, *436*(July), 5–8, doi:10.1038/nature03641.

Thomas, P., J. Veverka, S. Lee, and A. Bloom (1981), Classification of wind streaks on Mars, *Icarus*, *45*, 124–153.

Tirsch, D., R. Jaumann, A. Pacifici, and F. Poulet (2011), Dark aeolian sediments in Martian craters: Composition and sources, *J. Geophys. Res.*, *116*, E03002, doi:10.1029/2009JE003562.

Tsoar, H. (1983), Linear dunes—Forms and formation, *Prog. Phys. Geogr.*, *13*(4), 507–528, doi:10.1177/030913338901300402.

Tsoar, H. (2001), Types of aeolian sand dunes, in *Geomorphological Fluid Mechanics*, edited by N. Balmforth and A. Provenzale, pp. 403–429, Springer, Berlin.

Tucholke, B. E. (1982), Origin of longitudinal triangular ripples on the Nova Scotian continental rise, *Nature*, *296*.

Tyler, T. (1979), Laboratory studies of sand patterns resulting from current movements, in *Study of Global Sand Seas*, *USGS Prof. Pap. 1052*, edited by E. D. McKee, pp. 171–185.

Van Straaten, L. M. (1951), Longitudinal ripple marks in mud and sand, *J. Sediment. Petrol.*, *21*(1), 47–54.

Vaz, D. A., and S. Silvestro (2014), Mapping and characterization of small-scale aeolian structures on Mars: An example from the MSL landing site in Gale Crater, *Icarus*, *230*, 151–161, doi:10.1016/j.icarus.2013.08.007.

Veverka, J., P. Giearash, and P. Thomas (1981), Wind streaks on Mars: Meteorological control of occurrence and mode of formation, *Icarus*, *45*, 154–166.

Weitz, C. M., R. C. Anderson, J. F. Bell, W. H. Farrand, K. E. Herkenhoff, J. R. Johnson, B. L. Jolliff, R. V. Morris, S. W. Squyres, and R. J. Sullivan (2006), Soil grain analyses at Meridiani Planum, Mars, *J. Geophys. Res.*, *111*, E12S04, doi:10.1029/2005JE002541.

Werner, B. T., and G. Kocurek (1999), Bedform spacing from defect dynamics, *Geology*, *27*, 727–730, doi:10.1130/0091-7613(1999)027<0727.